Virtual Magnifying Glass Based on Optimal Mass Transportation

Chenxi Li

High School Affiliated to Zhejiang Normal University, Jinhua, Zhejiang

Abstract

In virtual reality/augmented reality (VR/AR) applications, especially medical image visualization, it is highly desirable to magnify region of interests. In this work, we propose a novel method for virtual magnifying glass for visualizing volumetric data based on Optimal Mass Transportation. An optimal mass transportation map deforms a volume to itself, transforms the source measure (volumetric element) to the target measure with the minimal transportation cost. Solving the optimal mass transportation problem is equivalent to a convex optimization, and can be converted to computing power Voronoi diagrams in classical computational geometry. The proposed method allows the user to accurately control the target measure, and select multiple regions of interests with irregular shapes. We demonstrate the effectiveness and efficiency of our method with several volume data sets from medical applications.

<<E59>>

1. Introduction

Recently virtual reality/augmented reality (VR/AR) technology has been applied for medical imaging. Doctors and surgeons are able to visualize medical images such as CT images, MRI images in the virtual environment for diagnosis or surgery planning. It is highly desirable to design a practical method to magnify the region of interest and allow the user to examine in details without losing the global view of the shape and the topology of the model. We propose a *virtual magnifying glass* technique for this purpose.

We can formulate this in a more formal way to further explain the idea. We use $\Omega \subset \mathbb{R}^3$ to denote the region with Euclidean volumetric element. The user assigns an importance function $\mu : \Omega \to \mathbb{R}^+$, which can be treated as the magnifying factor for the volumetric element. The deformation doesn't exceed the volume, therefore it is a self-mapping $\varphi : \Omega \to \Omega$. Furthermore, it is obvious that the mapping ϕ is smooth, one-to-one and onto, therefore φ should be a diffeomorphism. More importantly, the mapping deforms the initial Euclidean volumetric element to the target one,

$$D\varphi : dx \wedge dy \wedge dz \to \mu(x, y, z) dx \wedge dy \wedge dz$$

this requires the determinant of the Jacobian matrix of φ equals to μ,

$$\det(D\varphi)(x, y, z) = \mu(x, y, z). \tag{1}$$

1.1. *Optimal Mass Transportation Approach*

This work proposes a novel method for virtual magnifying glass based on Optimal Mass Transportation theory (OMT). Suppose the user gives a measure defined on Ω, which can be treated as the desired volumetric element, furthermore, assume the total measure equals to the initial volume. There are infinitely many diffeomorphsims which satisfy the Jacobian equation (1), but a unique one that minimizes the following transportation cost

$$C(\varphi) := \int_\Omega |p - \varphi(p)|^2 dxdydz,$$

where ϕ is the so-called *optimal mass transportation map*. Furthermore, there is a convex function $f : \Omega \to \mathbb{R}$, whose gradient map $p \mapsto \nabla f(p)$ gives the optimal mass transportation map. In this scenario, the Jacobian Eqn. (1) becomes the following *Monge-Amperé* equation

$$\det \, Hess \, f(x, y, z) = \mu(x, y, z),$$

where $Hess \, f$ is the Hessian matrix of the function f.

In our proposed approach, the Monge-Amperé equation is discretized and solved by a convex optimization. The optimization is iterative, at each step, and the algorithm boils down to computing the upper envelope of a set of hyper-planes, and projecting the envelope to obtain power Voronoi diagram and the dual power Delaunay triangulation, which can be carried out using classical algorithms in computational geometry [1].

Comparing to the existing methods, the OMT method has the following advantages: a) The exact solution to the Jacobian Eqn. (1) can be directly found, and the existence, uniqueness has theoretic guarantees. This allows the user to control the magnifying factor accurately; b) the OMT map is definitely a diffeomorphism, because its Jacobian is positive everywhere; c) the method to find the OMT map is equivalent to a convex optimization process. Due to the convexity of the energy, there is a unique global minimum. The result is independent of the initial condition, hence the method is easy to be reproduced.

2. Theoretic Background

In this section, we briefly introduce the theoretic foundation of our framework.

<<E59>>

2.1. *Optimal Mass Transportation*

Monge's Problem. Let X and Y be two metric spaces with probability measures μ and ν respectively. Assume X and Y have equal total measures:

$$\int_X \mu = \int_Y \nu.$$

A map $T : X \to Y$ is *measure preserving* if for any measurable set $B \subset Y$, the following condition holds:

$$\int_{T^{-1}(B)} \mu = \int_B \nu.$$

If this condition is satisfied, we say the push forward measure of μ induced by T equals to ν, and denote it as $\nu = T_{\#}\mu$.

Let $c(x, y)$ be the transportation cost for transporting $x \in X$ to $y \in Y$, then the total *transportation cost* of T is given by:

$$E(T) := \int_X c(x, T(x))\mu(x)dx. \tag{2}$$

In 18th century, Monge [2] raised the *optimal mass transportation problem*: how to find a measure preserving map T, $T_{\#}\mu = \nu$, that minimizes the transportation cost in Eqn. (2).

In the 1940s, Kantorovich [3] has introduced the relaxation of Monge's problem and solved it using linear programming. At the end of 1980's, Brenier [4] has proved the following theorem.

Theorem 1 [Brenier]. *Suppose X, Y are subsets in $\mathbb{R}^n$, the source X is a convex domain, the transportation cost is the quadratic Euclidean distance,*

$$c(x, y) = |x - y|^2.$$

Given probabilities measures μ and ν on X and Y respectively, then there is a unique optimal transportation map $T : (X, \mu) \to (Y, \nu)$, furthermore there is a convex function $f : X \to \mathbb{R}$, unique up to a constant, and the optimal mass transportation map is given by the gradient map $T : x \mapsto \nabla f(x)$.

Assume the measures μ and ν are smooth, f is with second order smoothness, $f \in C^2(X, \mathbb{R})$, then if f is measure-preserving, then it satisfies the Monge-Amperé equation:

$$\det \begin{pmatrix} \frac{\partial f}{\partial x_1^2} & \frac{\partial f}{\partial x_1 \partial x_2} & \cdots & \frac{\partial f}{\partial x_1 \partial x_n} \\ \frac{\partial f}{\partial x_2 \partial x_1} & \frac{\partial f}{\partial x_2^2} & \cdots & \frac{\partial f}{\partial x_2 \partial x_n} \\ \vdots & \vdots & & \vdots \\ \frac{\partial f}{\partial x_n \partial x_1} & \frac{\partial f}{\partial x_n \partial x_2} & \cdots & \frac{\partial f}{\partial x_n^2} \end{pmatrix} = \frac{\mu}{\nu \circ \nabla f}. \tag{3}$$

In general, Monge-Amperé equation is highly non-linear, conventional finite element method is incapable of solving this type of partial differential equations. Instead, based on its geometric interpretation, we can solve it using variational approach, by a convex optimization.

2.2. *Discrete Optimal Mass Transportation*

In practice, we formulate the optimal transportation problem in the discrete setting by sampling the target domain into a discrete point set, when the sampling density goes to infinity, the discrete solutions converge to the smooth solution. Suppose μ has a compact support on X, define

$$\Omega = \text{Supp } \mu = \{x \in X | \mu(x) > 0\},$$

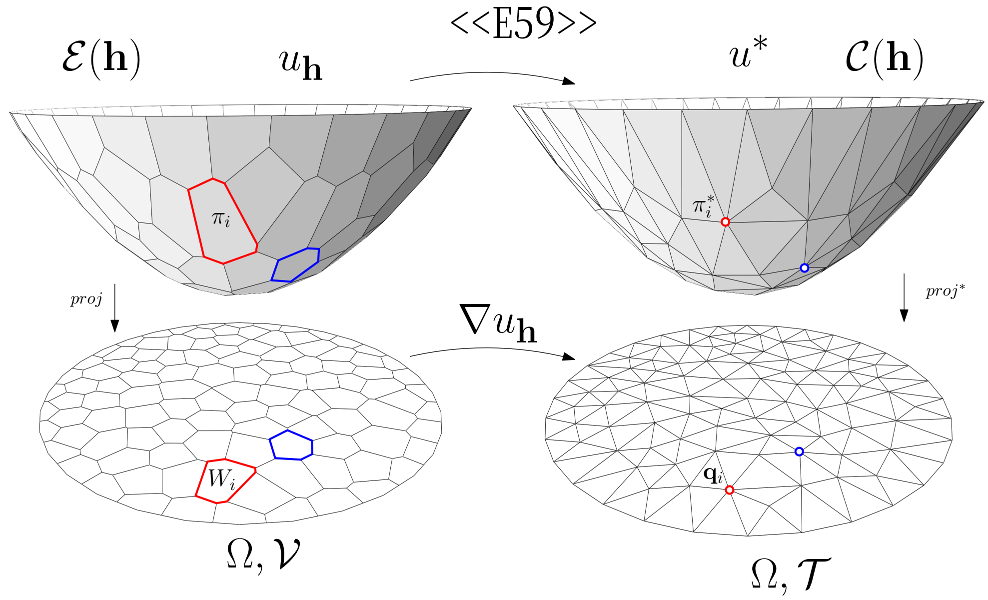

Fig. 1. The upper envelope $\mathcal{E}(\mathbf{h})$ of $\{\pi_i(\mathbf{h})\}$ is the dual to the convex hull $\mathcal{C}(\mathbf{h})$ of $\{\pi_i^*(\mathbf{h})\}$. The projection of $\mathcal{E}(\mathbf{h})$ induces the power Voronoi cell decomposition $\mathcal{V}(\mathbf{h})$ of Ω. The projection of $\mathcal{C}(\mathbf{h})$ induces the power Delaunay triangulation $\mathcal{T}(\mathbf{h})$ of the discrete samples $\{\mathbf{q}_i\}$. The upper envelope $\mathcal{E}(\mathbf{h})$ is the graph of a piecewise linear convex function $u_{\mathbf{h}}$. The gradient map of the convex function $\nabla u_{\mathbf{h}}$ maps each power Voronoi cell $W_i(\mathbf{h})$ to a sample point $\mathbf{q}_i$.

and assume Ω is a convex domain in X. The space Y is discretized into $Y = \{y_1, y_2, \cdots, y_k\}$ with Dirac measure

$$\nu = \sum_{i=1}^{k} v_i \delta(y - y_i).$$

We define a *height vector* $\mathbf{h} = (h_1, h_2, \cdots, h_k) \in \mathbb{R}^k$, consisting k real numbers. For each $y_i \in Y$, we construct a hyperplane defined on X:

$$\pi_i(\mathbf{h}) : \langle x, y_i \rangle + h_i = 0, \tag{4}$$

where $\langle , \rangle$ is the inner product in $\mathbb{R}^n$. Define a piece-wise linear function:

$$u_{\mathbf{h}}(x) = \max_{1 \le i \le k} \{\langle x, y_i \rangle + h_i\}, \tag{5}$$

then $u_{\mathbf{h}}$ is a convex function. We denote its graph by $G(\mathbf{h})$, which is an infinite convex polyhedron with supporting planes $\pi_i(\mathbf{h})$. Namely, $G(\mathbf{h})$ is the upper envelope of the planes $\{\pi_i(\mathbf{h})\}$. The projection of $G(\mathbf{h})$ induces a polyhedral partition of Ω,

$$\Omega = \bigcup_{i=1}^{k} W_i(\mathbf{h}),\ W_i(\mathbf{h}) := \{x \in X | u_{\mathbf{h}}(x) = \langle x, y_i \rangle + h_i\} \cap \Omega. \tag{6}$$

Each cell $W_i(\mathbf{h})$ is the projection of a facet of the convex polyhedron $G(\mathbf{h})$ onto Ω. The convex function $u_{\mathbf{h}}$ on each cell $W_i(\mathbf{h})$ is a linear function $\pi_i(\mathbf{h})$, therefore, the gradient map

$$\nabla u_{\mathbf{h}} : W_i(\mathbf{h}) \mapsto y_i,\ i = 1, 2, \cdots, k, \tag{7}$$

maps each cell $W_i(\mathbf{h})$ to a single point y_i.

The Brenier theorem 1 restricted on the current discrete setting can be formulated as follows:

<<E59>>

Theorem 2 [Discrete Optimal Mass Transport]. *For any given measures μ on X with convex support $\Omega \subset X$, and Dirac measure ν on Y, such that*

$$\int_\Omega d\mu = \sum_{i=1}^{k} \nu_i, \;\; \nu_i > 0,$$

there must exist a height vector $\mathbf{h}$ *unique up to adding a constant vector* $(c, c, \cdots, c)$, *the convex function in Eqn. (5) induces the cell decomposition of* Ω *as Eqn. (6), such that the following* measure-preserving *constraints are satisfied for all cells,*

$$\int_{W_i(\mathbf{h})} d\mu = \nu_i, \;\; i = 1, 2, \cdots, k. \tag{8}$$

Furthermore, the gradient map $\nabla u_\mathbf{h}$ *optimizes the following transportation cost*

$$E(T) := \int_\Omega |x - T(x)|^2 \mu(x) dx. \tag{9}$$

The existence and uniqueness have been first proven by Alexandrov [5] using a topological method. The existence has also been proven by Aurenhammer et al [6].

Recently, Gu et al. [1] have given a novel proof for the existence and uniqueness based on variational principle. First, we define the admissible space of the height vectors:

$$H := \{\mathbf{h} | \int_{W_i(\mathbf{h})} d\mu > 0\} \cap \{\sum_{i=1}^{k} h_i = 0\}. \tag{10}$$

Then, we define an energy $E(\mathbf{h})$ as the volume of the convex polyhedron bounded by the graph $G(\mathbf{h})$ and the cylinder through the boundary of Ω and minus a linear term,

$$E(\mathbf{h}) = \int_\Omega u_\mathbf{h}(x)\mu(x)dx - \sum_{i=1}^{k} \nu_i h_i. \tag{11}$$

The gradient of the energy is given by:

$$\nabla E(\mathbf{h}) = \left(\int_{W_i(\mathbf{h})} \mu - \nu_i \right). \tag{12}$$

Suppose the cells $W_i(\mathbf{h})$ and $W_j(\mathbf{h})$ intersect at a face

$$f_{ij}(\mathbf{h}) = W_i(\mathbf{h}) \cap W_j(\mathbf{h}) \cap \Omega,$$

then the Hessian of $E(\mathbf{h})$ is given by:

$$\frac{\partial^2 E(\mathbf{h})}{\partial h_i \partial h_j} = \begin{cases} \frac{\int_{f_{ij}(\mathbf{h})} \mu}{|y_j - y_i|}, & W_i(\mathbf{h}) \cap W_j(\mathbf{h}) \cap \Omega \neq \emptyset \\ 0, & otherwise. \end{cases} \tag{13}$$

It has been proven that the admissible space H is convex, and the Hessian matrix is positive definite on H, therefore the energy $E(\mathbf{h})$ is convex in Eqn.(11). Furthermore, the global unique minimum $\mathbf{h}^*$ is an interior point of H. At the minimum point, $\nabla E(\mathbf{h}^*) = 0$. This implies the gradient map $\nabla u_\mathbf{h}$ meets the measure-preserving constraint in Eqn. (8), furthermore the gradient map is the optimal mass transportation map.

Due to the convexity of the volume energy (Eqn.11), the global minimum can be obtained efficiently using Newton's method. Comparing to Kantorovich's approach, where there are k^2 unknowns, this approach has only k unknowns.

<<E59>>

3. Computational Algorithm

In the current work, the source domain Ω is the canonical unit cube in $\mathbb{R}^3$, the target is a set of discrete points $Y = \{\mathbf{q}_1, \mathbf{q}_2, \cdots, \mathbf{q}_k\}$ which densely and uniformly samples the unit cube. The source measure on the cube is the uniform measure $\mu = 1$ everywhere. The target measure on Y is prescribed by the user, $\nu = \{\nu_1, \nu_2, \cdots, \nu_k\}$.

For each target point $\mathbf{q}_i \in Y$, we construct a hyperplane in $\mathbb{R}^4$,

$$\pi_i(\mathbf{h}, \mathbf{p}) := \langle \mathbf{q}_i, \mathbf{p} \rangle + h_i, i = 1, 2, \cdots, k.$$

Then we compute the *upper envelope* of these hyper-planes $G(\mathbf{h})$.

Power Voronoi Diagram and Power Delaunay Triangulation. For each hyperplane $\pi_i(\mathbf{h})$, we construct a dual point $\pi_i^*(\mathbf{h}) \in \mathbb{R}^4$ as follows: assume the coordinates of $\mathbf{q}_i \in \mathbb{R}^3$ are (x_i, y_i, z_i), then the dual point is

$$\pi_i^*(\mathbf{h}) = (x_i, y_i, z_i, -h_i), i = 1, 2, \cdots, k.$$

Then we compute the *convex hull* of $\{\pi_1^*(\mathbf{h}), \pi_2^*(\mathbf{h}), \cdots, \pi_k^*(\mathbf{h})\}$ using incremental convex hull algorithm as described in [7], and denote the resulting convex hull as $\mathcal{C}(\mathbf{h})$.

We examine each tetrahedron t_{ijkl}on the boundary of the convex hull $\mathcal{C}(\mathbf{h})$ in $\mathbb{R}^4$,

$$t_{ijkl}(\mathbf{h}) \in \partial\mathcal{C}(\mathbf{h}).$$

The hyperplane equation of the tetrahedron is given by

$$\begin{vmatrix} x_i & y_i & z_i & -h_i & 1 \\ x_j & y_j & z_j & -h_j & 1 \\ x_k & y_k & z_k & -h_k & 1 \\ x_l & y_l & z_l & -h_l & 1 \\ x & y & z & w & 1 \end{vmatrix} = 0,$$

from this equation, we can obtain the normal to the hyperplane, denoted as $\mathbf{n}_{ijkl}$. If the w-component of the normal $\mathbf{n}_{ijkl}$ is negative, then we project the tetrahedron t_{ijkl} onto the (x, y, z)-hyperplane. This projection process of the convex hull $\mathcal{C}(\mathbf{h})$ produces a *power Delaunay* triangulation of the point set Y, denoted as $\mathcal{T}(\mathbf{h})$.

The upper envelope of the hyperplanes $\{\pi_i(\mathbf{h})\}$ is denoted as $\mathcal{E}(\mathbf{h})$, which is the dual to the lower part of the convex hull $\mathcal{C}(\mathbf{h})$. For each tetrahedron t_{ijkl} on the boundary of the convex hull $\partial\mathcal{C}(\mathbf{h})$, whose normal vector is with the negative w-component, its dual is a vertex on the upper envelope $\mathcal{E}(\mathbf{h})$, which is the intersection among 4 hyperplanes $\{\pi_i(\mathbf{h}), \pi_j(\mathbf{h}), \pi_k(\mathbf{h}), \pi_l(\mathbf{h})\}$. Each triangle Δ_{ijk} in the tetrahedron t_{ijkl} is dual to an edge in $\mathcal{E}(\mathbf{h})$, which is the intersection of 3 hyperplanes $\{\pi_i(\mathbf{h}), \pi_j(\mathbf{h}), \pi_k(\mathbf{h})\}$. Each edge e_{ij} in the tetrahedron t_{ijkl} corresponds to a face in $\mathcal{E}(\mathbf{h})$, which is the intersection of 2 hyperplanes $\{\pi_i(\mathbf{h}), \pi_j(\mathbf{h})\}$. Each vertex v_i in the tetrahedron t_{ijkl} corresponds to a cell in $\mathcal{E}(\mathbf{h})$, which is the cell supported by the hyperplane $\pi_i(\mathbf{h})$. By computing the dual of the convex hull $\mathcal{C}(\mathbf{h})$, we obtain the upper envelope $\mathcal{E}(\mathbf{h})$. We project the upper envelope onto the (x, y, z)-hyperplane to obtain the *power Voronoi diagram* of the hyperplane, each power Voronoi cell intersects Ω to obtain the power Voronoi cell decomposition of Ω, denoted as $\mathcal{V}(\mathbf{h})$.

In fact, the upper envelope $\mathcal{E}(\mathbf{h})$ is exactly the graph of the convex function $G(\mathbf{h})$, the power Voronoi diagram $\mathcal{V}(\mathbf{h})$ is the polyhedral partition of Ω by projecting $G(\mathbf{h})$ in Eqn. (6). The 2D analogy is depicted in Figure 1, which illustrates the upper envelope $\mathcal{E}(\mathbf{h})$, the convex hull $\mathcal{C}(\mathbf{h})$, the power Voronoi cell decomposition $\mathcal{V}(\mathbf{h})$, the power Delaunay triangulation $\mathcal{T}(\mathbf{h})$ and their relations for 2D case. Our current work focuses on the 3D case, which share the same principle but is hard to directly visualized.

Optimal Transportation Map. In our current setting, the discrete point set Y is contained in the unit cube

<<E59>>

Ω. The initial height vector is set as follows:

$$h_i = \frac{1}{2}\langle \mathbf{q}_i, \mathbf{q}_i \rangle, \ i = 1, 2, \cdots, k.$$

The initial power Delaunay triangulation $\mathcal{T}(\mathbf{h})$ is the traditional Delaunay triangulation, the power Voronoi cell decomposition of the unit cube $\mathcal{V}(\mathbf{h})$ is the traditional Voronoi cell decomposition.

At each step, we compute the power Delaunay triangulation $\mathcal{T}(\mathbf{h})$ and the power Voronoi cell decomposition $\mathcal{V}(\mathbf{h})$. The gradient of the volume energy in Eqn. (11) is given in Eqn. (12), the Hessian of the volume energy is given by Eqn. (13). Then we solve the following linear equation

$$\nabla E(\mathbf{h}) = \left(\frac{\partial^2 E(\mathbf{h})}{\partial h_i \partial h_j}\right) \delta\mathbf{h} \tag{14}$$

with the linear constraint $\sum_{i=1}^{k} h_i = 0$, the solution exists and is unique. Then we can update the height vector by using Newton's method

$$\mathbf{h} \leftarrow \mathbf{h} + \lambda(\delta\mathbf{h}),$$

where λ is the step length parameter. In theory, the step length parameter should be chosen such that the height vector is kept inside the admissible space H (Eqn.10), namely, in the power Voronoi cell decomposition $\mathcal{V}(\mathbf{h})$, each cell $W_i(\mathbf{h})$ is non-empty. In practice, in the middle of the optimization, we allow $\mathbf{h}$ to exceed the admissible space H. The convexity of the volume energy automatically guides the height vector to return to the admissible space. The details of the algorithm can be found in Alg.1.

4. Visualization

The volume raw image data is of resolution $512 \times 512 \times 512$, the range of the intensity of each voxel is from 0 to 255. The source domain Ω is the cube with side length 2, centered at the origin.

4.1. *ROI Selection and Target Measure Prescription*

The region of interest (ROI) can be selected manually. A simple and direct way for manual selection is as follows: the user specifies two concentric spheres $S(c, r)$ and $S(c, R)$, $r < R$, and a parameter $\lambda \geq 1$. We compute the target measure function $\mu : \Omega \to \mathbb{R}$, which equals to 1 outside the bigger sphere $S(c, R)$ and equals to λ inside the smaller sphere $S(c, r)$. Furthermore μ is a harmonic function in the region between the two spheres, hence satisfies the following Laplace equation with Dirichlet boundary conditions:

$$\begin{cases} \Delta\mu(p) = 0, \ r < |p - c| < R \\ \mu(p) = \lambda, \qquad |p - c| \ = r \\ \mu(p) = 1, \qquad |p - c| = R \end{cases} \tag{15}$$

Then we normalize the target measure, we first compute the current total volume

$$V = \int_{\Omega} \mu(p) dp,$$

then scale the target measure by $4/V$, $\mu \leftarrow 4\mu/V$.

4.2. *Discretization*

Discretize the Target Domain. In our algorithm, the target domain is discretized into a set of points $Y = \{\mathbf{q}_1, \mathbf{q}_2, \cdots, \mathbf{q}_k\}$. We use Delaunay refinement algorithm [1] to triangulate Ω, by specifying the maximal volume of each tetrahedron, we can obtain a uniform samplings. In practice, we use Tetgen [8] to compute the tetrahedron mesh of Ω. The tetrahedron mesh is still denoted as $\Omega = (V, E, F, T)$, where V, E, F, T represent the vertex, edge, face and tetrahedron set respectively. We use v_i to denote a vertex, e_{ij} and edge connecting v_i and v_j, t_{ijkl} a tetrahedron formed by v_i, v_j, v_k and v_l in the order.

<<E59>>

Discretize the Target Measure. The focus region can be selected by the user, two triangle meshes are chosen which approximate the two spheres. By abusing the symbols, the inner and outer spheres are still denoted as $S(c,r)$ and $S(c,R)$. The discrete Laplace-Beltrami operator is formulated using finite element method [9]. Suppose $e_{ij} \in E$ is an edge, then the *cotangent edge weight* is defined as

$$w_{ij} = \frac{1}{12} \sum_{kl} l_{kl} \cot \theta_{ij}^{kl}, \tag{16}$$

where l_{kl} represents the length of edge e_{kl}, θ_{ij}^{kl} the dihedral angle on the edge e_{kl} in the tetrahedron t_{ijkl}, the summation goes through all tetrahedra adjacent to the edge e_{ij}.

The target measure μ is approximated by a piecewise linear function, represented as a function defined on the vertex set, $\mu : V \to \mathbb{R}$, and is linearly interpolated for interior points. Namely, suppose p is a point inside a tetrahedron t_{ijkl}, then

$$\mu(p) = \lambda_i \mu(v_i) + \lambda_j \mu(v_j) + \lambda_k \mu(v_k) + \lambda_l \mu(v_l), \tag{17}$$

where $(\lambda_i, \lambda_j, \lambda_k, \lambda_l)$ is the *bary-centric coordinates* of p with respect to v_i, v_j, v_k, v_l, which is the unique solution satisfying the following linear equations:

$$\begin{cases} \lambda_i v_i + \lambda_j v_j + \lambda_k v_k + \lambda_l v_l = p \\ \lambda_i + \lambda_j + \lambda_k + \lambda_l \qquad\qquad = 1 \end{cases}$$

Then the discrete Laplace-Beltrami operator is

$$\Delta \mu(v_i) = \sum_{e_{ij} \in E} w_{ij} (\mu(v_j) - \mu(v_i)).$$

The smooth Laplace Eqn. (15) can be discretized to a linear equation system. It can be shown that the discrete Laplace-Beltrami operator is a positive definite matrix on the linear space $\sum_i x_i = 0$, therefore, the discrete Laplace equation has a solution unique up to a constant.

After obtaining the initial measure $\mu : V \to \mathbb{R}$, we calculate the total measure

$$V = \int_{\Omega} \mu(p) dp = \sum_{t_{ijkl}} \int_{t_{ijkl}} \mu(p) dp.$$

Because μ is piecewise linear, the integration of μ on each tetrahedron has a simple formula

$$\int_{t_{ijkl}} \mu(p) dp = \frac{1}{4} (\mu(v_i) + \mu(v_j) + \mu(v_k) + \mu(v_l)) Vol(t_{ijkl}). \tag{18}$$

Then we normalize the target curvature by $\mu \leftarrow 1/V \mu$. We compute the Voronoi cell decomposition of Ω using the vertices as the centers,

$$\Omega = \bigcup_{i=1}^{k} W_i, \quad W_i = \{ p \in \Omega | |p - v_i| \leq |p - v_j|, j = 1, 2, \cdots, k \}.$$

Then we compute the Dirac measure

$$\mu_j = \int_{W_j} \mu(p) dp.$$

The integration is computed as follows: we compute intersection between the Voronoi cell W_i and each tetrahedron t_{ijkl} in the Delaunay triangulation, the intersection is a convex polyhedron; we then decompose the convex polyhedron into a couple of tetrahedra, and compute the integration of μ on each tetrahedron using the formula in Eqn. (18). This process gives the Dirac measures for the samples $\{(v_1, \mu_1), (v_2, \mu_2), \cdots, (v_k, \mu_k)\}$.

4.3. *Optimal Mass Transportation Map* <<E59>>

The discrete optimal mass transportation map algorithm Alg.1 computes a power Voronoi cell decomposition of Ω, each cell $W_i(\mathbf{h})$ is mapped to a sample point v_i. Then, we convert this representation to a piecewise linear map from the tetrahedral mesh Ω to itself. For each Voronoi cell $W_i(\mathbf{h})$, we decompose it into a couple of tetrahedra t_i^j, the mass center of each tetrahedron is the mean of its four vertices, and denoted as c_i^j. The mass center of $W_i(\mathbf{h})$ is given by

$$c_i(\mathbf{h}) = \frac{\sum_j c_i^j \mathrm{Vol}(t_i^j)}{\sum_j \mathrm{Vol}(t_i^j)}.$$

If $W_i(\mathbf{h})$ intersects the boundary of Ω, we project its mass center onto the boundary surface $\partial\Omega$, and replace the mass center $c_i(\mathbf{h})$ by the projection image.

The cube Ω is triangulated by the power Delaunay triangulation $\mathcal{T}(\mathbf{h})$, and the vertex positions are $c_i(\mathbf{h})$ in the source domain, and v_i in the target domain. The piecewise linear map $\varphi : (\Omega, \mathcal{T}(\mathbf{h})) \to (\Omega, \mathcal{T}(\mathbf{h}))$ maps each vertex from $c_i(\mathbf{h})$ to v_i, $\varphi(c_i(\mathbf{h})) = v_i$.

4.4. *Voxel Resampling*

In the current work, we perform trilinear voxel resampling. For example, suppose we are given a volume image data S, and would like to generate another volume image data T with different resolutions and volumetric measure using the optimal mass transportation map $\varphi : \Omega \to \Omega$. The volume image data is represented as a three dimensional array. For each voxel $T(i,j,k)$ in T, we locate its position p in Ω, and find the tetrahedron t_{pqrs} containing p, compute the barycentric coordinates $(\lambda_p, \lambda_q, \lambda_r, \lambda_s)$ using Eqn. (17), then the preimage of p is given by

$$\varphi^{-1}(p) = \lambda_p c_p(\mathbf{h}) + \lambda_q c_q(\mathbf{h}) + \lambda_r c_r(\mathbf{h}) + \lambda_s c_s(\mathbf{h}),$$

then we find the voxels in S adjacent to $\varphi^{-1}(p)$, then use trilinear interpolation to get the intensity value of $\varphi^{-1}(p)$, and assign it to $T(i,j,k)$.

5. Experiments Results

We developed our system using generic C++ on a Windows platform, on a laptop with Dual Processor 2.9GHz CPU and 8GB Memory. The optimal mass transportation was implemented based on CGAL library for computing the power Voronoi diagram and Delaunay triangulation. The volumetric rendering was performed using Voreen based on raycasting algorithm with a GPU [10].

5.1. *Large Deformation and Global Smoothness*

Fig. 2 shows that our method is capable of designing large deformations and preserving the smoothness of the mapping. The volumetric Aneurism data is of resolution $256 \times 256 \times 256$. The focus region is the solid ball with center $c = (0.06, 0.32, 0.04)$ and radius $r = 0.1$. The magnifying factors are $1, 27, 125$, even as big as 343 in frame (d) which magnifies the volume of ROI by 343-fold. Because the optimal transportation map is the gradient map of a convex function, the Jacobian matrix of the OMT map is the Hessian matrix of the function. The Monge-Ameré equation in Eqn.(3) shows that the Jacobian is positive everywhere, therefore the OMT map is globally diffeomorphic.

5.2. *Smoothness of the Deformation*

The deformation for the whole volume is controlled by the continuity of the target measure as shown in Fig. 3. In the top row, the focus region is a solid ball centered at $c = (-0.42, 0.13, 0.26)$ and with radius $r = 0.26$. The target measure μ equals to $\lambda = 64$ inside the ball, and 1 outside the ball, hence μ is discontinuous.

<<E59>>

Algorithm 1: Volumetric Optimal Mass Transportation Map

Input: A convex domain $\Omega \subset \mathbb{R}^3$ and a set of discrete points $Y = \{\mathbf{q}_1, \cdots, \mathbf{q}_k\}$, discrete target measure $\nu = \{\nu_1, \cdots, \nu_k\}$, such that $\sum_i \nu_i = Vol(\Omega)$

Output: A partition of Ω, $\Omega = \cup_i W_i$, such that $W_i \mapsto \mathbf{q}_i$ is the optimal mass transportation map.

Translate and scale Y, such that $Y \subset \Omega$
Initialize the height vector $\mathbf{h}$, such that $h_i \leftarrow 1/2\langle \mathbf{q}_i, \mathbf{q}_i \rangle$
while *true* **do**
  for $i \leftarrow 1$ ***to*** k **do**
    Construct the hyperplane $\pi_i(\mathbf{h}) : \langle \mathbf{q}_i, \mathbf{p} \rangle + h_i$
    Compute the dual point of the hyperplane $\pi_i^*(\mathbf{h})$
  end
  Construct the convex hull $\mathscr{C}(\mathbf{h})$ of the dual points $\{\pi_i^*(\mathbf{h})\}$
  Compute the dual of the convex hull to obtain the upper envelope $\mathscr{E}(\mathbf{h})$ of the hyperplanes $\{\pi_i(\mathbf{h})\}$
  Project $\mathscr{C}(\mathbf{h})$ to obtain the power Delaunay triangulation $\mathscr{T}(\mathbf{h})$ of Y
  Project $\mathscr{E}(\mathbf{h})$ to obtain the power Voronoi cell decomposition $\mathscr{V}(\mathbf{h})$ of Ω
  for $i \leftarrow 1$ ***to*** k **do**
    Compute the volume of $W_i(\mathbf{h})$, denoted as $w_i(\mathbf{h})$
  end
  Construct the gradient $\nabla E(\mathbf{h}) = (\nu_i - w_i(\mathbf{h}))^T$
  for *each edge* $e_{ij} \in \mathscr{T}(\mathbf{h})$ **do**
    Compute the area of the dual face f_{ij}, denoted as A_{ij}
  end
  Construct the Hessian matrix $\partial^2 E(\mathbf{h})/\partial h_i \partial h_j = A_{ij}/|\mathbf{q}_j - \mathbf{q}_i|$
  Solve the linear equation $\text{Hess}(\mathbf{h})\delta\mathbf{h} = \nabla E(\mathbf{h})$
  $\lambda \leftarrow 1$
  Compute the power Voronoi diagram $\mathscr{V}(\mathbf{h} + \lambda\delta\mathbf{h})$ of Ω
  while $\exists w_i(\mathbf{h} + \lambda(\delta\mathbf{h})$ *is empty* **do**
    $\lambda \leftarrow 1/2\lambda$
    Compute the power Voronoi diagram $\mathscr{V}(\mathbf{h} + \lambda\delta\mathbf{h})$ of Ω
  end
  $\mathbf{h} \leftarrow \mathbf{h} + \lambda\delta\mathbf{h}$
  if $\forall |w_i(\mathbf{h}) - \nu_i| < \varepsilon$ **then**
    Break
  end
end
return *the mapping* $\{W_i(\mathbf{h}) \mapsto \mathbf{q}_i, i = 1, 2, \cdots, k\}$

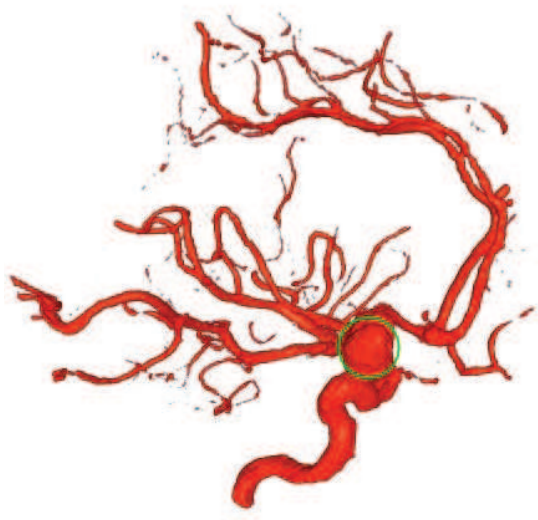

(a) $\lambda = 1$;

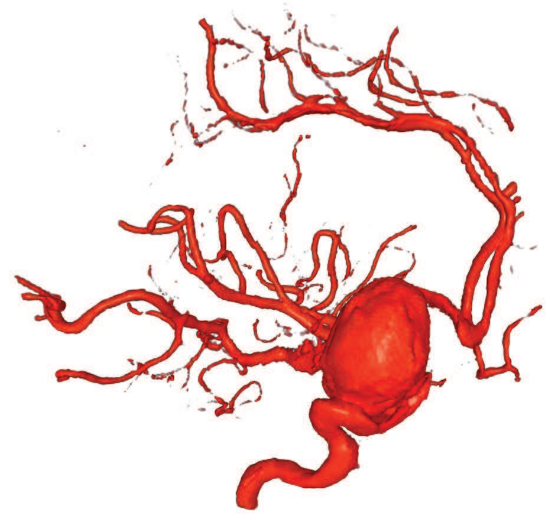

(b) $\lambda = 27$;

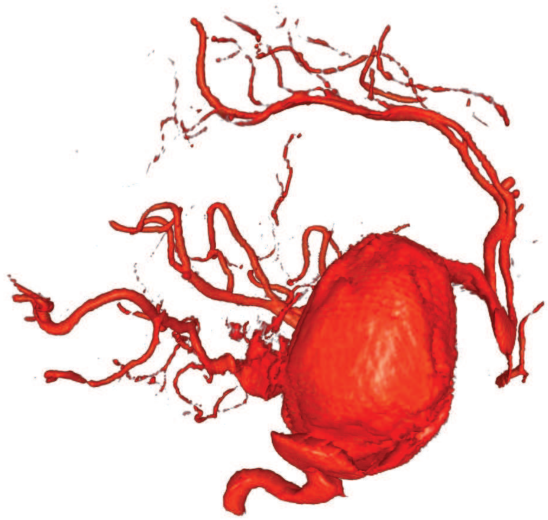

(c) $\lambda = 125$;

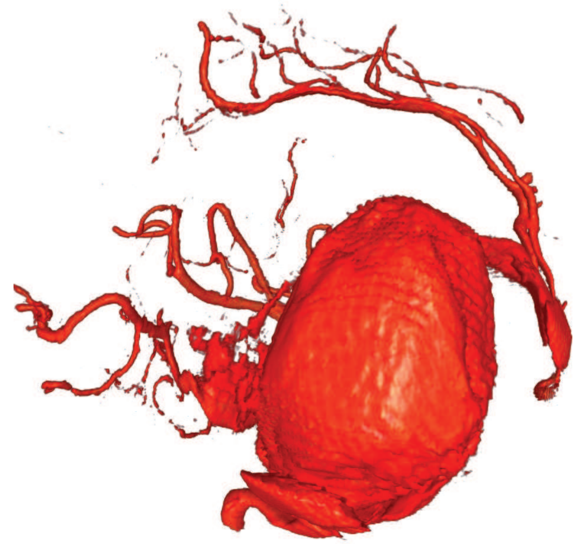

(d) $\lambda = 343$;

Fig. 2. The volumetric Aneurism is magnified by large scales using the OMT technique.

As shown in the top frames, this measure induces large deformations, especially at the boundary of the focus region. In the bottom row, we select two concentric balls, the center is $c = (-0.42, 0.13, 0.26)$, two radii are $r = 0.15$ and $R = 0.26$. The target μ equals $\lambda = 64$ inside the inner sphere, and 1 outside the outer sphere, and is a harmonic function between the two spheres. Therefore, μ is a smooth function. The deformation induced by the harmonic μ is prominently smaller, as shown in the bottom row. This demonstrates that the global deformation of the volume is greatly affected by the smoothness of the target measure.

<<E59>>

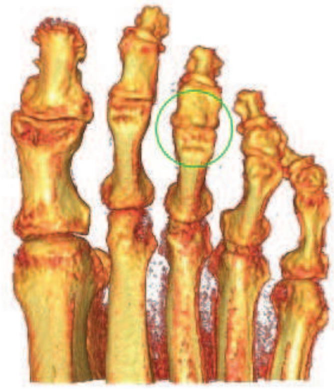

$(a)\lambda = 1;$

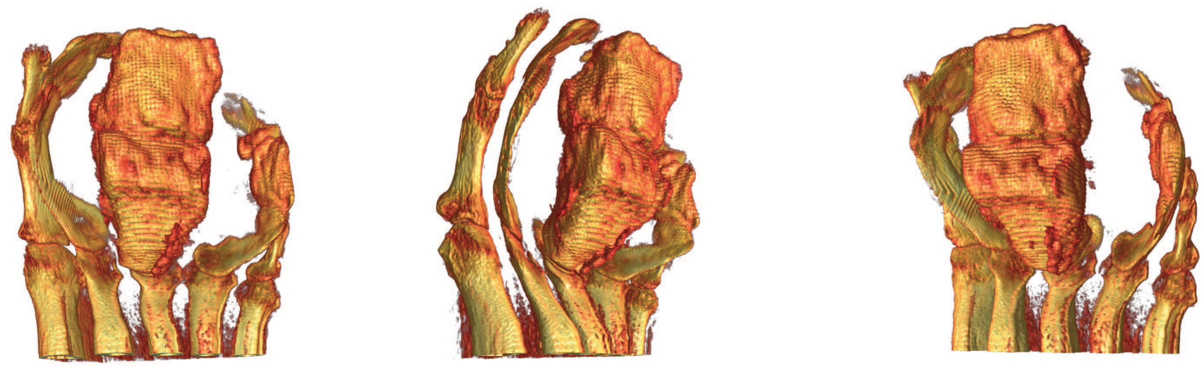

(b)Non-harmonic, front view; (c)Non-harmonic, left side view; (d)Non-harmonic, right side view;

(e) Harmonic,front view; (f)Harmonic, left side view; (g)Harmonic, right side view;

Fig. 3. The smoothness of the deformation is affected by the smoothness of the target measure μ. The μ is discontinuous for the left column; μ is harmonic for the right column.

5.3. *Irregular Region of Interests*

Fig. 4 shows that our algorithm allows the user to define highly irregular regions of interests. Instead of being regular solid balls, the focus region is a concave irregular shape encapsulating the vertebral column, toughly fitting to the content of interests in the volumetric data. The optimal mass transportation map is

<<E59>>

still diffeomorphic and has full control of the target measure.

5.4. *Multiple Focus Regions*

Our OMT based approach allows user to select multiple regions of interest, furthermore different regions of interests can be assigned with different magnifying factors. In the CT knee model given in Fig. 5, we select two regions of interests : one is the left patella region, the ball with center $c_1 = (-0.4, -0.36, -0.50)$, radius 0.19 and the magnifying factor $\lambda_1 = 8$; the other is the right tibia, the solid ball with center $c_2 = (0.46, -0.06, -0.71)$, radius 0.15 and the magnifying factor $\lambda_2 = 16$. Different frames show the visualization results with different views.

5.5. *Time Complexity*

We report the computational time in the Table 1. The volume Ω is a canonical cube with edge length 2. The number of discrete samples is about $10k$. The user manually selects the regions of interests, and the computation of the optimal mass transportation map is performed off line.

Table 1. Running time

Dataset	Data source	Running time	resolution
Aneurism	Philips Research, Hamburg,Germany	118s	$512 \times 512 \times 512$
Foot	Philips Research, Hamburg,Germany	182s	$256 \times 256 \times 256$
NCAT phantom	Segars WP, Tsui BMW	156s	$512 \times 512 \times 512$
CT knee	Department of Radiology University of Iowa	134s	$440 \times 440 \times 440$

6. Conclusion

This work introduces a virtual magnifying glass method for medical image visualization based on Optimal Mass Transportation theory, which guarantees the existence, uniqueness and smoothness of the solution. It allows the user to accurately control the target volumetric element, select multiple focus regions with irregular shapes. The method can be implemented using power Voronoi diagram and Delaunay triangulation in classical computational geometry. Furthermore, the method can be generalized to higher dimensions.

Currently, the computation of the method is not in real time. In the future, we will implement the optimal mass transformation map algorithms on GPU to improve the speed, and generalize the visualization technique to higher dimensional data.

<<E59>>

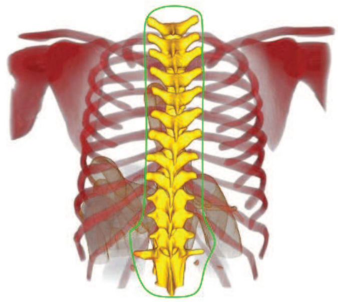

(a) Original model, front view;

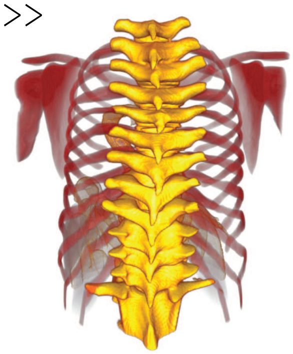

(b) $\lambda = 27$, front view;

(c) Original model, left view;

(d) $\lambda = 27$, left view;

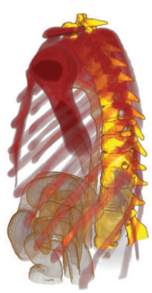

(e) Original model, right view;

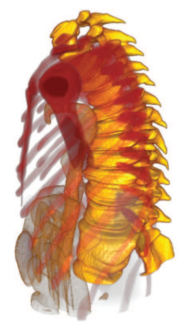

(f) $\lambda = 27$, right view;

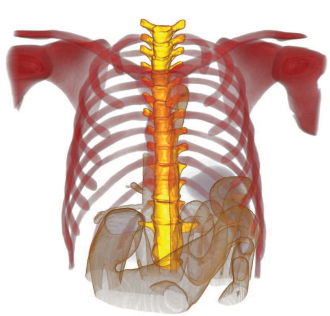

(g) Original model, back view;

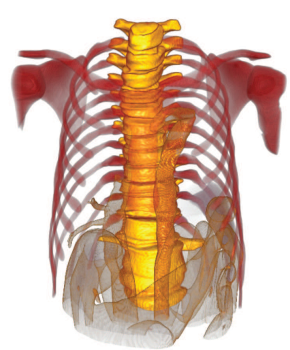

(h) $\lambda = 27$, back view;

Fig. 4. Visualization for NCAT phantom model, the regions of interest are irregular shapes.

<<E59>>

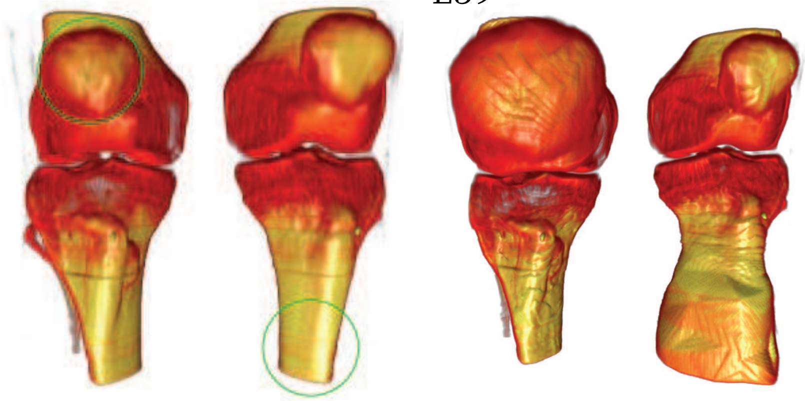

(a) Original model, front view; (b) $\lambda_1 = 8, \lambda_2 = 16$, front view;

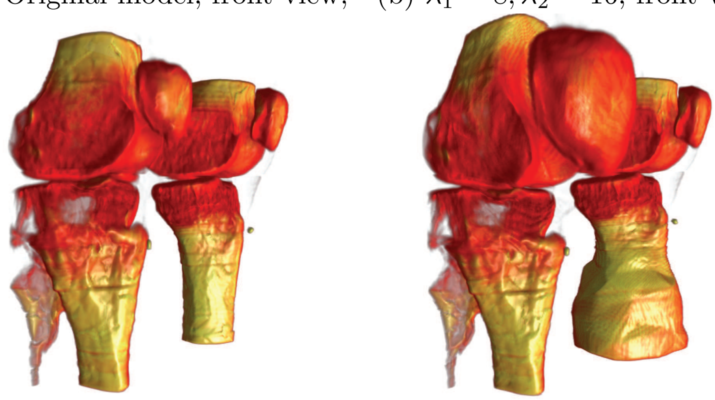

(c) Original model, side view; (d) $\lambda_1 = 8, \lambda_2 = 16$, side view;

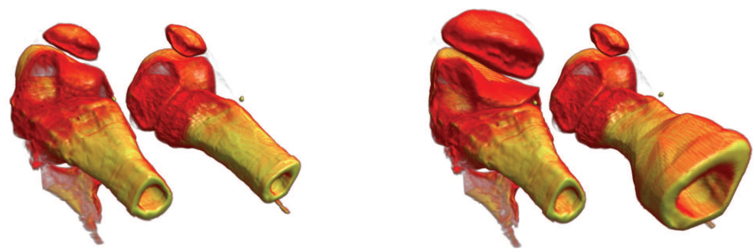

(e) Original model, bottom view;(f) $\lambda_1 = 8, \lambda_2 = 16$, bottom view;

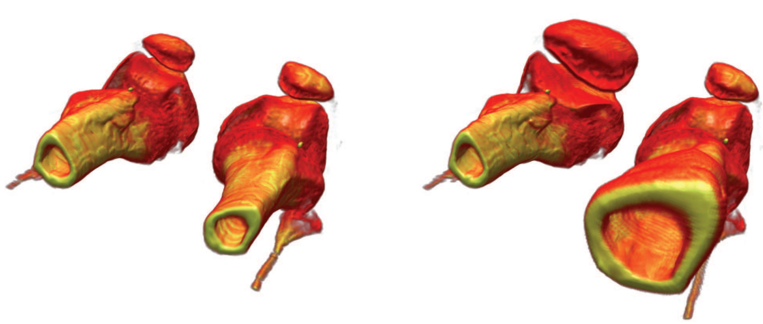

(g) Original model, side view; (h) $\lambda_1 = 8, \lambda_2 = 16$,side view;

Fig. 5. Visualization for CT Knee model with multiple focus magnification in different views.

<<E59>>

References

[1] X. Gu, F. Luo, J. Sun, S.-T. Yau, Variational principles for minkowski type problems, discrete optimal transport, and discrete monge-ampere equations, Asian Journal of Mathematics(AJM) 2 (20) (2016) 383C398.

[2] N. Bonnotte, From knothes rearrangement to breniers optimaltransport map, arX1 95 iv:1205.1099 [math.OC].

[3] L. Kantorovich, On a problem of monge, Uspekhi Mat. Nauk. 3 (1948) 225C226.

[4] Y. Brenier, Polar factorization and monotone rearrangement of vectorvalued functions, Comm. Pure. Appl. Math. 44 (4).

[5] A. D. Alexandrov, Convex polyhedra, Springer Monographs in Mathematics. 200 Springer-Verlag, Berlin.

[6] F. Aurenhammer, Power diagrams: properties, algorithms and applications, SIAM Journal on Computing 16 (1) (1987) 78C96.

[7] M. de Berge, O. Cheong, M. van Kreveld, M. Overmars, Computational Geometry: Algorithm and Application, 3rd Edition, Springer-Verlag, 2008.

[8] H. Si, Tetgen, a delaunay-based quality tetrahedral mesh generator, ACM Transactions on Mathematical Software 41 (2) (2015) Article No.: 11. DOI: 10.1145/2629697 http://dl.acm.org/10.1145/2629697.

[9] M. Reuter, F.-E. Wolter, N. Peinecke, Laplace-beltrami spectra as shape-dna of surfaces and solids, Computer-Aided Design 38 (4) (2006) 342C366.

[10] J. Meyer-Spradow, T. Ropinski, J. Mensmann, K. H. Hinrichs, Voreen: A rapidprototyping environment for ray-casting-based volume visualizations, IEEE Computer Graphics and Applications (Applications Department) 29 (6) (2009) 6C13.
URL http://viscg.uni-muenster.de/publications/2009/MRMH09